

Absorption Tails of Donor:C₆₀ Blends Provide Insight into Thermally Activated Charge-Transfer Processes and Polaron Relaxation

Koen Vandewal,^{*,†} Johannes Benduhn,[†] Karl Sebastian Schellhammer,^{‡,§} Tim Vangerven,^{||} Janna E. Rückert,^{‡,§} Fortunato Piersimoni,[⊥] Reinhard Scholz,[†] Olaf Zeika,[†] Yeli Fan,^{#,||} Stephen Barlow,[#] Dieter Neher,[⊥] Seth R. Marder,[#] Jean Manca,⁷ Donato Spoltore,[†] Gianaurelio Cuniberti,^{‡,§,||} and Frank Ortman^{*,‡,§}

[†]Dresden Integrated Center for Applied Physics and Photonic Materials (IAPP) and Institute for Applied Physics, [‡]Institute for Materials Science, Max Bergmann Center of Biomaterials and Dresden Center for Computational Materials Science, and [§]Center for Advancing Electronics Dresden (cfaed), Technische Universität Dresden, 01062 Dresden, Germany

^{||}Material Physics Division, Institute for Materials Research (IMO-IMOMECE), Hasselt University, Universitaire Campus, Wetenschapspark 1, B-3590 Diepenbeek, Belgium

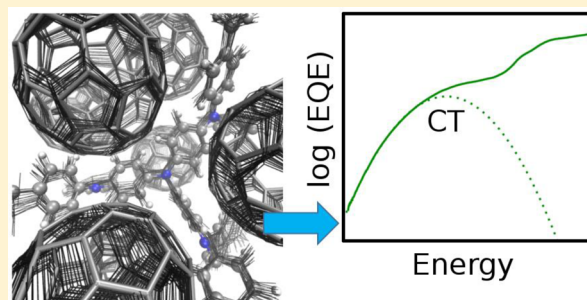
[⊥]Institute of Physics and Astronomy, University of Potsdam, Karl-Liebknecht-Straße 24-25, 14476 Potsdam, Germany

[#]Center for Organic Photonics and Electronics and School of Chemistry and Biochemistry, Georgia Institute of Technology, Atlanta, Georgia 30332-0400, United States

⁷X-Lab, Hasselt University, Universitaire Campus, Agoralaan 1, B-3590 Diepenbeek, Belgium

Supporting Information

ABSTRACT: In disordered organic semiconductors, the transfer of a rather localized charge carrier from one site to another triggers a deformation of the molecular structure quantified by the intramolecular relaxation energy. A similar structural relaxation occurs upon population of intermolecular charge-transfer (CT) states formed at organic electron donor (D)–acceptor (A) interfaces. Weak CT absorption bands for D–A complexes occur at photon energies below the optical gaps of both the donors and the C₆₀ acceptor as a result of optical transitions from the neutral ground state to the ionic CT state. In this work, we show that temperature-activated intramolecular vibrations of the ground state play a major role in determining the line shape of such CT absorption bands. This allows us to extract values for the relaxation energy related to the geometry change from neutral to ionic CT complexes. Experimental values for the relaxation energies of 20 D:C₆₀ CT complexes correlate with values calculated within density functional theory. These results provide an experimental method for determining the polaron relaxation energy in solid-state organic D–A blends and show the importance of a reduced relaxation energy, which we introduce to characterize thermally activated CT processes.



INTRODUCTION

Electron-transfer events are ubiquitous in organic optoelectronic devices such as organic light-emitting diodes, solar cells, and photodetectors. A proper description of these electron-transfer processes has to take into account the soft nature of solid organic semiconductors and the relatively weak intermolecular electronic coupling, which in turn generally results in localization of charge carriers accompanied by a deformation of the molecular structure. The relaxation energy (Λ) is an important parameter because it quantifies these effects in terms of resulting energy gain from the geometry change upon charging of the molecular entity. For instance, for intermolecular electron transfer, the sum of the Λ values of the reactants defines the reorganization energy of the electron-transfer reaction. Values for Λ are often obtained using simulations based on density functional theory for single

chromophores.^{1,2} Experimental validation of Λ values, calculated as such, for thin films of neat or blended organic semiconductors is however rare but necessary to verify and eventually improve theoretical models.³

Important fundamental processes in organic electronic devices depend on Λ . For example, an accurate prediction of the charge-carrier mobility and its thermal activation in amorphous organic thin films depends crucially on Λ , which determines the barrier that charge carriers have to overcome to move to neighboring molecular sites, as described by Marcus theory and its extensions.^{4,5} Furthermore, structural relaxation at electron donor (D)–electron acceptor (A) interfaces affects the energies of the involved electronic levels and, thus, the

Received: December 14, 2016

Published: January 10, 2017

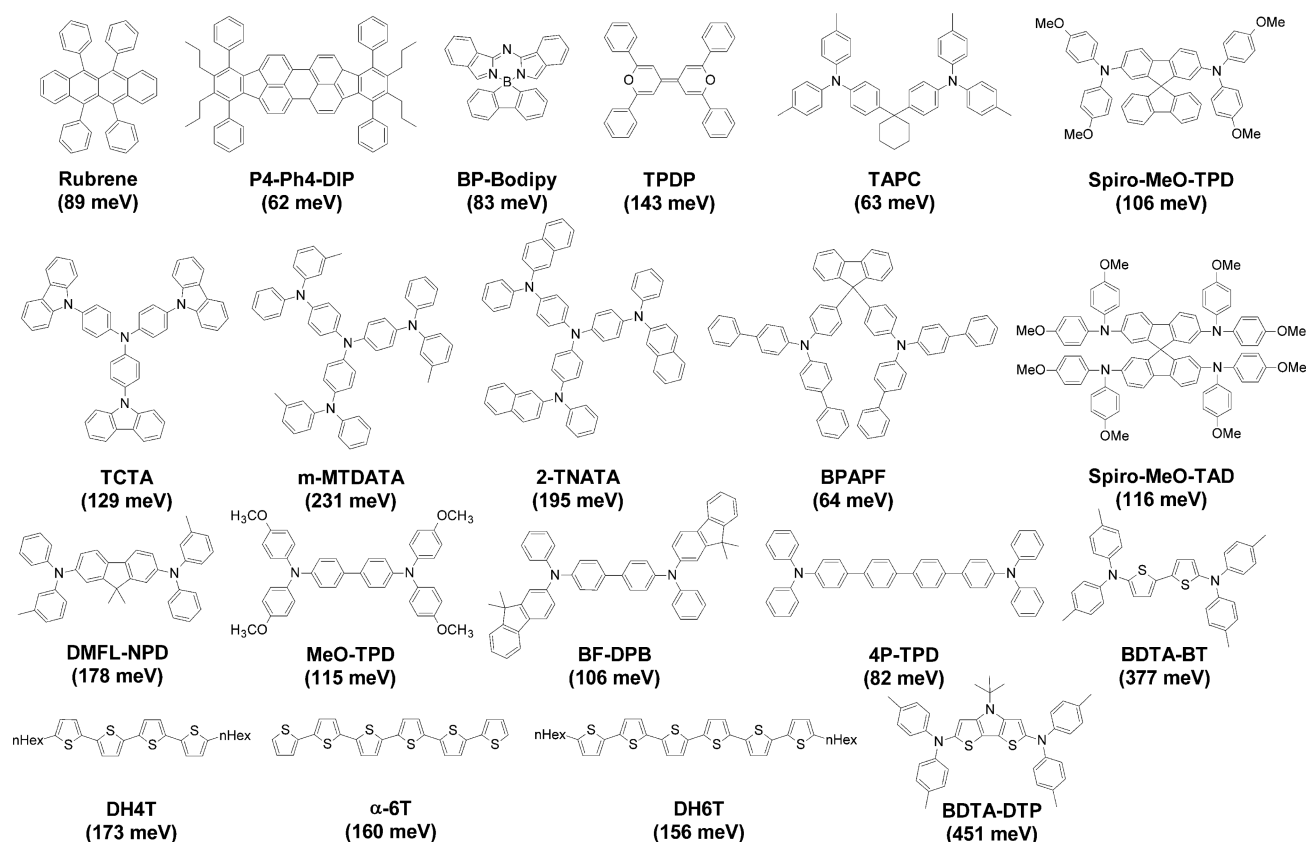


Figure 1. Chemical structures of the molecules used in this study. Their calculated relaxation energies Λ_D ranging from 62 to 451 meV are provided in parentheses.

photoinduced electron-transfer process. The latter is important for the generation of free charges in organic solar cells and photodetectors. In particular, for devices with a low driving force for the formation of a charge-transfer (CT) state from a localized D or A state, an associated high Λ will reduce the free-carrier generation rate.^{6,7}

Photogeneration and recombination of charge carriers at D–A interfaces typically involve CT states.⁸ These intermolecular electronic states lead to additional weak absorption and emission in the spectral region below the optical gaps of both the D and A. Optical excitation spectra of these states are broad and often featureless.⁸ In analogy to amorphous inorganic semiconductors, the absorption tail of the CT absorption band is sometimes taken as a quantitative measurement of the corresponding inhomogeneous broadening by the energetic distribution of localized states of the donor material.^{9–11} However, it is unclear if this approach is valid because additional absorption tail broadening arises from thermal population of higher energy vibrational levels of the ground state.¹² At room temperature, the latter effect might dominate.

In this work, we investigate the absorption tails of CT states for a large set of 20 different electron-donating molecules diluted at a molar ratio of 6% in the electron acceptor C_{60} . Within this series, the line width of CT absorption varies over a wide range and depends strongly on the donor material used. We show that thermally activated molecular movement is the main effect responsible for the variation in the steepness of the CT absorption tail. Importantly, this effect is quantified by the relaxation energy $\Lambda_{DA}^{\text{exp}}$ of the CT state. Experimental values for $\Lambda_{DA}^{\text{exp}}$ determined from slope fitting correlate with the polaron relaxation energy Λ_D of the donor molecule calculated using

density functional theory. However, a *reduced relaxation energy* Λ_D' , in which high-frequency vibrational modes are omitted, has a closer physical correspondence and fits better to the measured quantity for low- Λ compounds in which there is strong coupling of the CT excitation to a high-frequency mode. Thus, our work introduces a new experimental method to estimate the reduced relaxation energy of the donor molecules in solid-state organic devices.

RESULTS AND DISCUSSION

We investigate 20 hole-transporting molecular materials whose chemical structures are given in Figure 1. These materials are coevaporated in a low (6 mol %) molar ratio with C_{60} , forming 50 nm films. The use of such a low donor content minimizes the effects of donor aggregation, simplifying the analysis and theoretical calculations.

All materials are electron donors with a relatively high optical gap, forming CT states at energies below the optical gap of C_{60} (<1.8 eV). To spectrally resolve CT absorption bands, we perform ultrasensitive measurements of the external quantum efficiency (EQE) spectrum of photovoltaic diodes comprising the diluted D: C_{60} blends (see the Methods section for more experimental details). Spectra for exemplary D: C_{60} combinations are shown in Figure 2.

The CT absorption tails for all investigated D: C_{60} blends have a Gaussian line shape. The spectral position and width of the CT absorption band depend strongly on the donor material used. For example, the CT state of rubrene: C_{60} has a rather steep onset, whereas the tail of m-MTDATA: C_{60} is much more shallow.

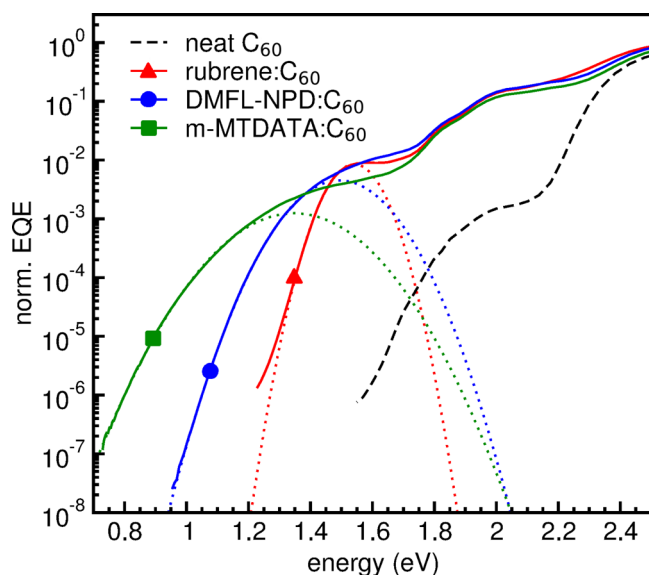


Figure 2. Normalized EQE spectra of exemplary D:C₆₀ blends. Spectra are normalized in the region of C₆₀ absorption around 2.5 eV. CT absorption occurs at photon energies below 1.75 eV, the optical gap of C₆₀. Gaussian fits to the CT absorption tails, according to eq 1, are plotted as dotted lines. C₆₀ absorption is indicated as a dashed line.

For the donors TAPC, 6T, BDTA-BT, and BDTA-DTP, we have investigated the influence of the D:C₆₀ mixing ratio. We observe only minor effects on the line shape of the CT absorption bands (see discussion in the Supporting Information and Figures S1 and S2). For 6T, which is known to easily aggregate, we observe a redshift of the CT band upon increasing donor concentrations above 20% (Figure S1). However, for concentrations below 20%, only minor concentration effects on the line shape are observed. Therefore, one can be confident that the use of 6 mol % of donor ensures the least influence of aggregation on the relaxation energy.

Furthermore, temperature-dependent measurements of the tail of TAPC:C₆₀ reveal that the width of the CT band decreases when lowering the temperature (see analysis in Figure S3). This implies that, at room temperature, optical transitions from the ground state to the CT state are assisted by thermally activated vibrations above the ground-state energy, thus determining the low-energy part of the CT absorption band. In this case, the CT absorption tails obey the following relation^{12,13}

$$\text{EQE}(E) \sim \exp\left(-\frac{(E - E_{\text{CT}} - \Lambda_{\text{DA}}^{\text{exp}})^2}{4\Lambda_{\text{DA}}^{\text{exp}}k_{\text{B}}T}\right) \quad (1)$$

where E_{CT} is the difference between the ground-state and CT-state energies in their respective equilibrium geometries, and $\Lambda_{\text{DA}}^{\text{exp}}$ is the relaxation energy related to the CT transition. The latter comprises both the relaxation of C₆₀ (energy Λ_{A}) and the relaxation of the donor (energy Λ_{D}), and the simplifying assumption of equal Λ values for charged and neutral states enters the derivation of eq 1. Potentially, there may be additional contribution from relaxation of the surrounding environment upon the introduction of a CT dipole field into the system. As donor molecules are diluted, the environment is mostly C₆₀ and, therefore, rather invariant for all D:C₆₀ samples studied.

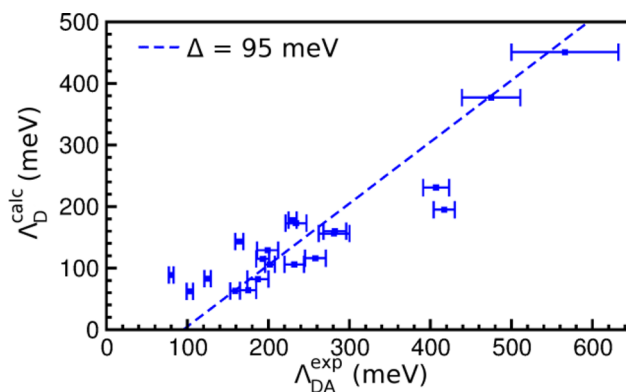


Figure 3. Comparison between experimentally obtained relaxation energy of the donor-C₆₀ CT state $\Lambda_{\text{DA}}^{\text{exp}}$ and the calculated relaxation energy of the donor $\Lambda_{\text{D}}^{\text{calc}}$. The dashed line represents eq 2 with $\Delta = 95$ meV. Experimental error bars indicate uncertainty of the Gaussian fit procedure (see Supporting Information for details).

Fitting the room temperature spectra with eq 1 yields experimental values $\Lambda_{\text{DA}}^{\text{exp}}$ for all D:C₆₀ combinations, spanning a large range from 80 meV for rubrene to 566 meV for BDTA-DTP (tabulated values in the Supporting Information). For comparison, we calculate relaxation energies for holes on single donor molecules, $\Lambda_{\text{D}}^{\text{calc}}$, using density functional theory at the B3LYP/6-311G** level of theory based on neutral and charged molecular geometries (see Methods section for details).^{1,2} Values $\Lambda_{\text{D}}^{\text{calc}}$ for each molecule can be found in Figure 1.

A central result of our study is contained in Figure 3, which shows a clear correlation between experimentally obtained $\Lambda_{\text{DA}}^{\text{exp}}$ and calculated $\Lambda_{\text{D}}^{\text{calc}}$ values. This result suggests that the large variation in width of the CT absorption band, over the range of investigated donor molecules, is primarily determined by differences in their internal relaxation energy Λ_{D} .

Therefore, the calculated relaxation energy relates to the experimentally determined relaxation energy according to

$$\Lambda_{\text{D}}^{\text{calc}} = \Lambda_{\text{DA}}^{\text{exp}} - \Delta \quad (2)$$

To further quantify this result, we determine the offset between $\Lambda_{\text{DA}}^{\text{exp}}$ and $\Lambda_{\text{D}}^{\text{calc}}$ in Figure 3 by a linear fit and obtain $\Delta = 95$ meV, which allows for establishing an empirical relationship among all studied donor materials. Even without detailed knowledge of the origin of Δ , this finding thus allows for a quite accurate prediction of the line width of CT absorption by simple calculations of $\Lambda_{\text{D}}^{\text{calc}}$ based on structural relaxation. The quality of the fit with eq 2 is given by a root-mean-square deviation of 54 meV.

If a higher accuracy is desired, a better understanding of the scattering of the results and of the origin of the offset is required. Moreover, by virtue of the analogy of thermally activated CT absorption in the tails and thermally activated electronic transport, deeper analysis of the results will lead to conclusions concerning the use of the relaxation energy for carrier-transport simulations. Both issues are addressed below.

We first note that the origin of Δ is partly related to the relaxation energy of C₆₀ (between C₆₀ anion geometry and its neutral equilibrium geometry) but may also contain contributions of the relaxation energy of the dielectric environment or static disorder. All of these contributions sum to Δ , and each is positive and expected to be significantly larger than zero. Hence, one expects $\Delta \geq \Lambda_{\text{A}} = 109$ meV.¹⁶ However, as is clear from Figure 3, there are a few materials for which Δ is less than

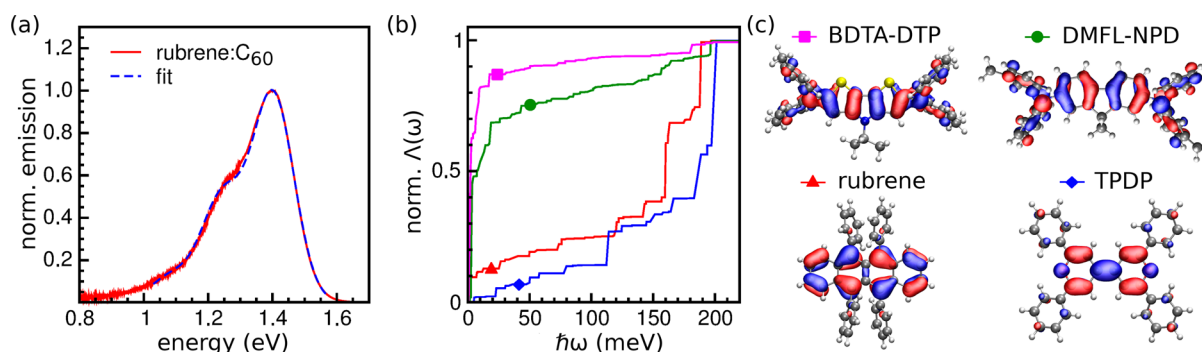


Figure 4. (a) CT emission spectrum of rubrene:C₆₀. (b) Mode-resolved contributions to the relaxation energy of exemplary donor materials. The cumulated relaxation energies $\Lambda(\omega)$ are calculated (see main text) and normalized to their maximum values at high frequencies. (c) Highest occupied molecular orbitals of donor molecules contained in (b).

50 meV or even negative, which at first glance seems physically impossible. These materials comprise stiff, small molecules, such as the donors TPDP ($\Delta = 21$ meV), P4-Ph-DIP ($\Delta = 41$ meV), BP-Bodipy ($\Delta = 42$ meV), and rubrene ($\Delta = -9$ meV).

For further elucidating this discrepancy, it is instructive to have a closer look to the experimentally obtained CT emission spectrum of rubrene:C₆₀ (Figure 4(a)) exemplary for these low $\Lambda_{\text{D}}^{\text{calc}}$ material systems. As opposed to CT emission for materials with a large $\Lambda_{\text{DA}}^{\text{exp}} > 200$ meV, the CT emission spectrum of rubrene:C₆₀ shows vibronic structure with several phonon replicas spaced at 160 meV. These phonon satellites indicate a quantum character of a single phonon mode or a group of modes and are similar to the satellites in gas-phase singlet absorption spectra for rubrene.¹⁴ In π -conjugated molecules, the spacing of approximately 160 meV stems from ring breathing modes that strongly couple to the electronic levels.¹⁵ The phonon replicas have a Gaussian line shape, and in analogy to the analysis of the absorption spectra, the high-energy tail of the CT emission spectrum can be fitted with a Gaussian, allowing an alternative extraction of $\Lambda_{\text{DA}}^{\text{exp}}$ (see also the Supporting Information). Values extracted from CT absorption (80 meV) and emission (88 meV) tails for rubrene:C₆₀ are similar. Absorption and emission spectra generally yield similar $\Lambda_{\text{DA}}^{\text{exp}}$ values.⁸

From the clear resolution of the replica structure in CT emission for rubrene:C₆₀, we conclude that the width of the absorption and emission tails is dominated by low-frequency modes, whereas the high-frequency modes determine the spacing between the different peaks of the CT emission (and absorption) spectrum.¹² To calculate the relaxation energy responsible for the broadening of the CT absorption tail, one should thus restrict the calculation of Λ_{D} to the low-frequency modes, as only those show significant temperature-dependence of their population at room temperature.

To distinguish these contributions, we calculate the mode-resolved relaxation energies Λ_j (mode index j) using the procedure described in ref 2. Many low- and high-frequency modes have finite Λ_j . A straightforward comparison is possible when summing these spectral contributions in cumulated relaxation energies defined as $\Lambda(\omega) = \sum_{\omega_j < \omega} \Lambda_j$. For large ω , one obtains the sum of all spectral contributions, which yields a value very similar to the relaxation energy obtained from direct relaxation calculations (see Methods section). Figure 4(b) presents the normalized $\Lambda(\omega)$ of some representative molecules whose molecular orbitals are shown in Figure 4(c).

We identify two different types of behavior: molecules with frontier orbitals extending to the flexible substituents exhibiting strong contributions from low-energy modes, as evidenced by a steep low-frequency rise in $\Lambda(\omega)$ for BDTA-DTP and DMFL-NPD; and in contrast, molecules such as rubrene and TPDP show dominant contributions for high-frequency modes. For such modes, it can be expected that they exhibit quantum features at room temperature because they satisfy the condition $\frac{\hbar\omega}{k_{\text{B}}T} \gg 1$. Although this condition does not provide a clear frequency cutoff, our analysis shows that in cases where the molecules are relatively stiff, strong electron–phonon coupling dominates the spectral region above 125 meV, which we choose as a practical cutoff. To quantify this effect, we define an *effective high-frequency mode*, which integrates the contribution of such modes to an effective relaxation energy $\Lambda_{\text{D}}^{\text{qm}} = \sum_{\hbar\omega_j > 125\text{meV}} \Lambda_j$. This effective mode (replacing the group of high-frequency modes and keeping their total relaxation energy) is a very convenient concept in the following discussion. Being a nonclassical mode, its contribution to the line width is not covered by eq 1. In contrast, by virtue of level quantization related to this mode, it eventually leads to a more discrete vibrational density of states as well as more pronounced phonon-replica structure and less thermal broadening in the spectra.

As a result, this effective quantum mode has to be removed from the calculation of the relaxation energy responsible for broadening the low-energy tail of the CT absorption. The remaining relaxation energy is thus smaller and denoted *reduced relaxation energy* henceforth ($\Lambda_{\text{D}}^{\text{calc}} = \Lambda_{\text{D}}^{\text{calc}} - \Lambda_{\text{D}}^{\text{qm}}$). We obtain large corrections for TPDP ($\Lambda_{\text{D}}^{\text{qm}} = 105$ meV, $\Lambda_{\text{D}}^{\text{calc}} = 38$ meV), P4-Ph-DIP ($\Lambda_{\text{D}}^{\text{qm}} = 48$ meV, $\Lambda_{\text{D}}^{\text{calc}} = 14$ meV), BP-Bodipy ($\Lambda_{\text{D}}^{\text{qm}} = 48$ meV, $\Lambda_{\text{D}}^{\text{calc}} = 43$ meV), and rubrene ($\Lambda_{\text{D}}^{\text{qm}} = 51$ meV, $\Lambda_{\text{D}}^{\text{calc}} = 38$ meV). Characteristic for these molecules are their small size and/or rigid nature, which favors the occurrence of quantum modes and hence absorption tails that are narrower than expected based on theoretical values of $\Lambda_{\text{D}}^{\text{calc}}$. In contrast, for the less stiff larger molecules with orbital contributions at flexible substituents such as DMFL-NPD ($\Lambda_{\text{D}}^{\text{qm}} = 31$ meV, $\Lambda_{\text{D}}^{\text{calc}} = 147$ meV) and BDTA-DTP ($\Lambda_{\text{D}}^{\text{qm}} = 29$ meV, $\Lambda_{\text{D}}^{\text{calc}} = 422$ meV), the corrections for the reduced relaxation energy are relatively small. For consistency, we apply the same procedure for C₆₀ and obtain ($\Lambda_{\text{D}}^{\text{qm}} = 71$ meV, $\Lambda_{\text{A}}^{\text{calc}} = 38$ meV) based on literature data.¹⁶

In Figure 5, the reduced relaxation energies of the CT pair $\Lambda_{\text{DA}}^{\text{calc}}$ are compared to the measured relaxation energies $\Lambda_{\text{DA}}^{\text{exp}}$. The removal of modes with quantum character leads to a better

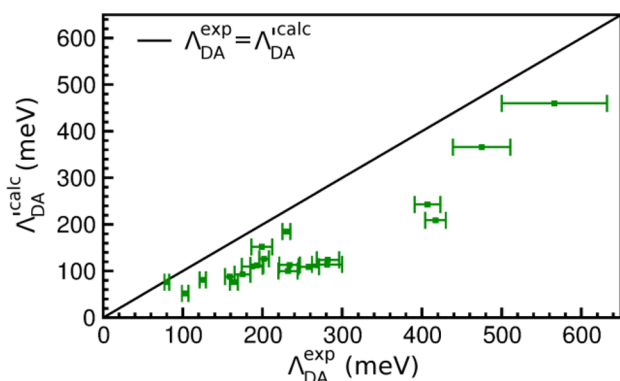


Figure 5. Correlation of the reduced donor–acceptor relaxation energy $\Lambda_{DA}^{\text{calc}}$ (the sum of the reduced relaxation energies of D and A, see main text) and experimental data $\Lambda_{DA}^{\text{exp}}$. The solid line indicates that the lower limit of $\Lambda_{DA}^{\text{exp}}$ is determined by the calculated reduced quantity.

fit of low- Λ materials to the overall trend of data points. It also resolves the unphysical result of negative Δ . Indeed, the solid line in Figure 5 shows that $\Lambda_{DA}^{\text{calc}}$ is a lower bound for $\Lambda_{DA}^{\text{exp}}$. We believe that in most cases the remaining offset between the two quantities is most likely due to the relaxation energy of the dielectric environment and inhomogeneous broadening, which might contribute to larger experimental relaxation, whose detailed contributions are the subject of future work. Finally, we note that the two data points in Figures 3 and 5 at around $\Lambda_{DA}^{\text{exp}} = 400$ meV stem from m-MTDATA and 2-TNATA, and their deviation from the linear relation is likely due to an overdelocalization of the positive charge in the DFT calculation for these particular molecules, resulting in an underestimation of calculated relaxation energies, as discussed in the Supporting Information.

The observation in Figure 5 that $\Lambda_{DA}^{\text{calc}} \leq \Lambda_{DA}^{\text{exp}}$ holds for all donors, whereas it was frequently violated for the full relaxation energies $\Lambda_{DA}^{\text{calc}}$, which indicates another implication of our work that is important to the low- Λ materials. These materials in particular are interesting from the viewpoint of high-mobility charge transport. The observation of an upper experimental limit for the thermally relevant relaxation energy Λ' in such organic materials, which is significantly smaller than the full molecular value Λ (compare Table S1), implies that for charge transport the same reduced relaxation energy is primarily responsible for the thermal activation effects.

Indeed, Marcus theory describes the strong influence of the relaxation energy on transport via thermal activation of initial configurations for electron-transfer events. In the present work, the same temperature activation is directly measured in CT-EQE spectroscopy, and we have observed that quantum modes have to be subtracted because their zero-point vibrational ground state does not contribute to thermal activation behavior, thus setting an upper limit for the appropriately reduced Λ' . Furthermore, this finding implies that only theoretical approaches, such as quantum-based electron-transfer or polaron-based transport approaches,⁵ that can describe this behavior should be used for transport simulations in such materials, whereas the use of the popular classical Marcus hopping rate appears inappropriate and is therefore discouraged. The results in Table S1 show that small and/or rigid molecules including C_{60} receive a strong quantum correction to the relaxation energy (between 48 and 77%). Although this correction is smaller for large- Λ compounds, we

expect the same strong effect on the reduced relaxation energies of similar high-mobility materials.

CONCLUSIONS

First, our work shows that, in the studied donor- C_{60} blends, low-frequency thermally activated intramolecular vibrations of donor molecules are the most important contributor to the CT absorption line shape at low photon energies, i.e., the line shape can be reasonably well described in terms of a Marcus-type expression and that static disorder does not play a major role. The magnitude of the relaxation energy of the CT state, extracted from the CT absorption tail, correlates with the calculated polaron relaxation energy of the single donor molecule. Although this finding can be used as a first empirical law for predicting the CT absorption line shape, an improved accuracy, relevant for stiff molecules with a small apparent experimental relaxation energy, is achieved by treating high-frequency modes quantum mechanically, leading to the introduction of a *reduced relaxation energy* Λ'_D . CT absorption (and emission) spectra can thus be used as a direct experimental measure of Λ'_D for donors in solid state, an important molecular parameter, e.g., for charge transport, and may thus be instrumental for improving theoretical models.

The use of sensitive techniques to measure absorption tails in organic materials is becoming increasingly popular to extract a disorder parameter related to charge transport.^{17,18} In this respect, our work emphasizes the importance of taking into account the impact of intramolecular vibrations and relaxation of polarons and excitons on the total energetic disorder of the organic semiconductor with high relevance for the generation and recombination of free charges in photodetectors and organic solar cells.

METHODS

Device Preparation. The photovoltaic devices are thermally evaporated at ultrahigh vacuum (base pressure $< 10^{-7}$ mbar) onto a glass substrate with a prestructured ITO contact (Thin Film Devices, USA). Two nanometers of MoO_3 are deposited to adjust the ITO work function to form an Ohmic hole contact. The “diluted donor” active layer comprises 50 nm of C_{60} (CreaPhyS GmbH, Germany) doped with 6 mol % of each donor molecule (for more details, see Table S1). Afterward, 8 nm of bathophenanthroline (BPhen, abcr GmbH, Germany), used as electron contact, is evaporated and finished with 100 nm of Al. The device is defined by the geometrical overlap of the bottom and the top contact with an active area of 6.44 mm². For exposure to ambient conditions to be avoided, the organic part of the device is covered by a small glass substrate glued on top.

Sensitive EQE Measurements. The light of a quartz halogen lamp (50 W) is chopped at 140 Hz and coupled into a monochromator (Cornerstone 260 1/m, Newport). The resulting monochromatic light is focused onto the solar cell; its current at short-circuit conditions is fed to a current preamplifier before it is analyzed with a lock-in amplifier (7280 DSP, Signal Recovery, Oak Ridge, USA). For a spectrum spanning over 5–7 decades to be achieved, the time constant of the lock-in amplifier was chosen to be 1 s, and the amplification of the preamplifier was increased to resolve low photocurrents. The EQE was determined by dividing the photocurrent of the organic solar cell by the flux of incoming photons, which was obtained with a calibrated silicon (Si) and/or indium–gallium–arsenide (InGaAs) photodiode.

Electroluminescence Measurements. These values were obtained with an Andor SR393i-B spectrometer equipped with a cooled Si and InGaAs detector array (DU420A-BR-DD, DU491A-1.7). The spectral response of the setup was calibrated with a reference lamp (Oriol 63355). The emission spectrum of the organic solar cell was recorded at different injection currents with respect to voltages

that were lower than or at least similar to the open-circuit voltage of the device at 1 sun illumination.

Theoretical Calculations. All calculations were performed within density functional theory using the Gaussian09 software package in combination with the B3LYP hybrid functional and the 6-311G** basis set.^{19–23} Relaxation energies of the donor molecules are obtained from the adiabatic potential energy surface of the neutral state according to $\Lambda_{\text{D}}^{\text{calc}} = E(q_+) - E(q_0)$, where $E(q_+)$ is the energy of the neutral molecule in the relaxed geometry of the cationic state, and $E(q_0)$ is the ground-state energy.

In mode-resolved calculations, each normal mode j contributes to the relaxation process according to a dimensionless electron–phonon coupling constant g_j with $\Lambda_{\text{D}}^{\text{calc}} = \sum_j \Lambda_j = \sum_j g_j^2 \hbar \omega_j$. The coupling constants g_j are extracted from an expansion of the relaxed neutral structure by the normal mode vectors followed by an evaluation of the linear variation in HOMO energy according to ref 2. Here, we apply a scaling factor of 0.967 for the frequencies of the vibrational modes $\hbar \omega_j$, but we maintain the relaxation energies Λ_j by increasing the coupling constants g_j by a factor of $\sqrt{1/0.967}$.²⁴

■ ASSOCIATED CONTENT

Supporting Information

The Supporting Information is available free of charge on the ACS Publications website at DOI: 10.1021/jacs.6b12857.

List of the investigated donor materials and their corresponding relaxation energies, temperature-dependent EQE measurements, analysis of the CT emission spectrum of rubrene:C₆₀, and further details of the computations (PDF)

■ AUTHOR INFORMATION

Corresponding Authors

*koen.vandewal@iapp.de

*frank.ortmann@tu-dresden.de

ORCID

Tim Vangerven: 0000-0003-1936-9521

Gianaurelio Cuniberti: 0000-0002-6574-7848

Present Address

[†]Y.F.: School of Chemistry and Chemical Engineering, Southeast University, Nanjing 211189, Jiangsu, P.R. China

Notes

The authors declare no competing financial interest.

■ ACKNOWLEDGMENTS

This work was supported by the German Federal Ministry for Education and Research (BMBF) through the InnoProfile project “Organische p-i-n Bauelemente 2.2”. F.O. would like to thank the German Research Foundation (DFG) for financial support (Grant OR 349/1). This work was partly supported by the DFG within the Cluster of Excellence “Center for Advancing Electronics Dresden.” F.P. and D.N. acknowledge funding by the DFG via the SFB 951 “HIOS”. T.V. acknowledges the Agency for Innovation by Science and Technology in Flanders (IWT) for funding his Ph.D. The work at Georgia Tech was supported by the Department of the Navy, Office of Naval Research Award No. N00014-14-1-0580 (CAOP MURI) and through a state-sponsored scholarship for graduate students to Y.F. from the China Scholarship Council. We acknowledge the Center for Information Services and High Performance Computing (ZIH) at TU Dresden for computational resources. We thank Prof. Bäuerle from the University of Ulm for the supply of DH4T and DH6T and Markus Hummert for P4-Ph4-DIP and BP-Bodipy.

■ REFERENCES

- (1) Coropceanu, V.; Cornil, J.; da Silva Filho, D. A.; Olivier, Y.; Silbey, R.; Brédas, J. L. *Chem. Rev.* **2007**, *107*, 926.
- (2) Ortmann, F.; Radke, K. S.; Günther, A.; Kasemann, D.; Leo, K.; Cuniberti, G. *Adv. Funct. Mater.* **2015**, *25*, 1933.
- (3) Kera, S.; Ueno, N. *J. Electron Spectrosc. Relat. Phenom.* **2015**, *204*, 2.
- (4) Marcus, R. A. *Rev. Mod. Phys.* **1993**, *65*, 599. Marcus, R. A.; Sutin, N. *Biochim. Biophys. Acta, Rev. Bioenerg.* **1985**, *811*, 265.
- (5) Holstein, T. *Ann. Phys.* **1959**, *8*, 343. Levich, V. G. *Adv. Electrochem. Electrochem. Eng.* **1966**, *4*, 249. Kestner, N. R.; Logan, J.; Jortner, J. *J. Phys. Chem.* **1974**, *78*, 2148.
- (6) Coffey, D. C.; Larson, B. W.; Hains, A. W.; Whitaker, J. B.; Kopidakis, N.; Boltalina, O. V.; Strauss, S. H.; Rumbles, G. *J. Phys. Chem. C* **2012**, *116*, 8916.
- (7) Ward, A. J.; Ruseckas, A.; Kareem, M. M.; Ebenhoch, B.; Serrano, L. A.; Al-Eid, M.; Fitzpatrick, B.; Rotello, V. M.; Cooke, G.; Samuel, I. D. *Adv. Mater.* **2015**, *27*, 2496.
- (8) Vandewal, K. *Annu. Rev. Phys. Chem.* **2016**, *67*, 113.
- (9) Street, R. A.; Song, K. W.; Northrup, J. E.; Cowan, S. J. *Phys. Rev. B: Condens. Matter Mater. Phys.* **2011**, *83*, 165207.
- (10) Street, R. A.; Krakaris, A.; Cowan, S. R. *Adv. Funct. Mater.* **2012**, *22*, 4608.
- (11) Samiee, M.; Joshi, P.; Aidarkhanov, D.; Dalal, V. *Appl. Phys. Lett.* **2014**, *105*, 133511.
- (12) Gould, I. R.; Noukakis, D.; Gomez-Jahn, L.; Young, R. H.; Goodman, J. L.; Farid, S. *Chem. Phys.* **1993**, *176*, 439.
- (13) Marcus, R. A. *J. Phys. Chem.* **1989**, *93*, 3078.
- (14) Heinemeyer, U.; Scholz, R.; Gisslén, L.; Alonso, M. I.; Ossó, J. O.; Garriga, M.; Hinderhofer, A.; Kytka, M.; Kowarik, S.; Gerlach, A.; Schreiber, F. *Phys. Rev. B: Condens. Matter Mater. Phys.* **2008**, *78*, 085210.
- (15) Gisslén, L.; Scholz, R. *Phys. Rev. B: Condens. Matter Mater. Phys.* **2009**, *80*, 115309.
- (16) Faber, C.; Janssen, J. L.; Côté, M.; Runge, E.; Blase, X. *Phys. Rev. B: Condens. Matter Mater. Phys.* **2011**, *84*, 155104.
- (17) Kronemeijer, A. J.; Pecunia, V.; Venkateshvaran, D.; Nikolka, M.; Sadhanala, A.; Moriarty, J.; Szumilo, M.; Sirringhaus, H. *Adv. Mater.* **2014**, *26*, 728.
- (18) Venkateshvaran, D.; Nikolka, M.; Sadhanala, A.; Lemaire, V.; Zelazny, M.; Kepa, M.; Hurhangee, M.; Kronemeijer, A. J.; Pecunia, V.; Nasrallah, I.; Romanov, I.; Broch, K.; McCulloch, I.; Emin, D.; Olivier, Y.; Cornil, J.; Beljonne, D.; Sirringhaus, H. *Nature* **2014**, *515*, 384.
- (19) Frisch, M. J.; Trucks, G. W.; Schlegel, H. B.; Scuseria, G. E.; Robb, M. A.; Cheeseman, J. R.; Scalmani, G.; Barone, V.; Mennucci, B.; Petersson, G. A.; Nakatsuji, H.; Caricato, M.; Li, X.; Hratchian, H. P.; Izmaylov, A. F.; Bloino, J.; Zheng, G.; Sonnenberg, J. L.; Hada, M.; Ehara, M.; Toyota, K.; Fukuda, R.; Hasegawa, J.; Ishida, M.; Nakajima, T.; Honda, Y.; Kitao, O.; Nakai, H.; Vreven, T.; Montgomery, J. A., Jr.; Peralta, J. E.; Ogliaro, F.; Bearpark, M.; Heyd, J. J.; Brothers, E.; Kudin, K. N.; Staroverov, V. N.; Kobayashi, R.; Normand, J.; Raghavachari, K.; Rendell, A.; Burant, J. C.; Iyengar, S. S.; Tomasi, J.; Cossi, M.; Rega, N.; Millam, J. M.; Klene, M.; Knox, J. E.; Cross, J. B.; Bakken, V.; Adamo, C.; Jaramillo, J.; Gomperts, R.; Stratmann, R. E.; Yazyev, O.; Austin, A. J.; Cammi, R.; Pomelli, C.; Ochterski, J. W.; Martin, R. L.; Morokuma, K.; Zakrzewski, V. G.; Voth, G. A.; Salvador, P.; Dannenberg, J. J.; Dapprich, S.; Daniels, A. D.; Farkas, Ö.; Foresman, J. B.; Ortiz, J. V.; Cioslowski, J.; Fox, D. J. *Gaussian 09*, revision D.01; Gaussian, Inc.: Wallingford, CT, 2009.
- (20) Becke, A. D. *Phys. Rev. A: At., Mol., Opt. Phys.* **1988**, *38*, 3098.
- (21) Becke, A. D. *J. Chem. Phys.* **1993**, *98*, 1372.
- (22) Becke, A. D. *J. Chem. Phys.* **1993**, *98*, 5648.
- (23) Krishnan, R.; Binkley, J. S.; Seeger, R.; Pople, J. A. *J. Chem. Phys.* **1980**, *72*, 650.
- (24) Scott, A. P.; Radom, L. *J. Phys. Chem.* **1996**, *100*, 16502.